Materials Science in Semiconductor Processing 68 (2017) 165–171

Contents lists available at ScienceDirect

Materials Science in Semiconductor Processing

journal homepage: www.elsevier.com/locate/mssp

Electrochemical properties of $BiFeO_3$ nanoparticles: Anode material for sodium-ion battery application

Lignesh Durai[a,1], Brindha Moorthy[b,1], Collin Issac Thomas[a], Do Kyung Kim[b,*], K. Kamala Bharathi[a,*]

[a] Department of Physics and Nanotechnology, SRM University, Research Institute, Kattankulathur, Chennai 603203, India
[b] Department of Materials Science and Engineering, Korea Advanced Institute of Science and Technology (KAIST), 291 Daehak-ro, Yuseong-gu, Daejeon 34141, Republic of Korea

ARTICLE INFO

Keywords:
Anode material
Nanoparticle
Cyclic voltammetry
Charge discharge
$BiFeO_3$

ABSTRACT

We report on synthesis and possibilities of utilizing $BiFeO_3$ (BFO) nanoparticles and bulk materials as an anode component for sodium (Na) ion batteries. XRD and Raman spectroscopy measurements shows that as synthesized BFO exhibits rhombohedrally distorted perovskite structure. Cyclic voltammetry (CV) reveals that conversion redox mechanism takes place at first discharge and subsequently two alloying process. The specific capacity of BFO bulk material is seen to be 650 mAh/g at first cycle and gradually decreases to 250 mAh/g after 30 cycles (0.1 C rate). After 30 cycles, capacity fading takes place very slowly and is observed to be 180 mAh/g at 100th cycle. The discharge capacity of BFO material at different current rates is carried out and the better performance is seen at the current rates of 25 mA/g. The conversion reaction mechanism during the electrochemical reaction in $BiFeO_3$ is probed by combining ex-situ XRD and XPS measurements after electrochemical cycling. CV of BFO nanoparticles exhibit very stable performance. Whereas, the charge discharge curve shows similar capacity fading as the bulk BFO. High initial capacity of $BiFeO_3$ gives an indication that it can be utilized as an anode component for Na ion batteries after stabilizing the capacity fading.

1. Introduction

Over the past thirty years, Li ion batteries (LIB's) are extensively used in wide range of portable electronic and electrical devices such as cell phones, laptops and desktop computers to most of the electrical vehicles (EVs) [1–5]. On the other hand, rarity of Li resources is key drawback to power EVs which need large scale production [6]. Hence, it is very essential to find alternate battery technology that can replace Li as a main source. Na is a very promising candidate with redox potential −2.71 V and holds similar chemistry with Li and much abundant throughout the world [6]. Sodium ion batteries (SIB's) could replace LIB's in small as well as large-scale energy storage applications [7,8]. Substantial progress has been achieved by several research groups in the search of cathode materials for SIB's by utilizing the knowledge gained from LIB's [9,10]. Graphite, the well-studied and commercialized anode material of LIB's cannot be employed for SIB's due to its low capacity [11].

Many metal oxides and Sb based on conversion reaction anode materials have been investigated by several research groups such as Co_3O_4, NiO, Mn_3O_4, Fe_3O_4, MoO_3, Sb_2O_3 and Sb_2O_4 [12–17]. Above mentioned metal oxides based anode materials with electrochemically inactive metal element display the low capacities (less than 500 mAh/g) or capacity fading effect. Whereas, Sb based materials are reported to have stable cyclability and moderate capacity [18]. High initial capacity of 580 mAh/g and subsequent reduction to 260 mAh/g after 50 cycles is reported for the SnO thick films [19]. Metal sulfides are also well explored anode materials, suffers due to large volume expansion [20]. Various titanium-based compounds such as $Na_2Ti_6O_{13}$, $Na_2Ti_3O_7$ and $Na_4Ti_5O_{12}$ have been reported as promising anode materials for SIB's [21–23]. However, low Na storage site and low specific capacity of these materials limits their application.

In the search of new anode material for SIB's, we have examined the structural and electrochemical properties of $BiFeO_3$ bulk and nanomaterial. Perovskite $BiFeO_3$ (BFO) is a well-known multiferroic material, which exhibits antiferromagnetic ordering and ferroelectric ordering at ambient temperature [24]. BFO undergoes a ferroelectric (FE) and antiferromagnetic transitions (Neel temperature (T_N)) at 1103 K and 643 K respectively [25–28].

* Corresponding author.
E-mail addresses: dkkim@kaist.ac.kr (D. Kyung Kim), kamalabharathi.k@ktr.srmuniv.ac.in (K. Kamala Bharathi).
[1] Equal Contribution.

http://dx.doi.org/10.1016/j.mssp.2017.06.003
Received 11 April 2017; Received in revised form 10 May 2017; Accepted 3 June 2017
Available online 16 June 2017

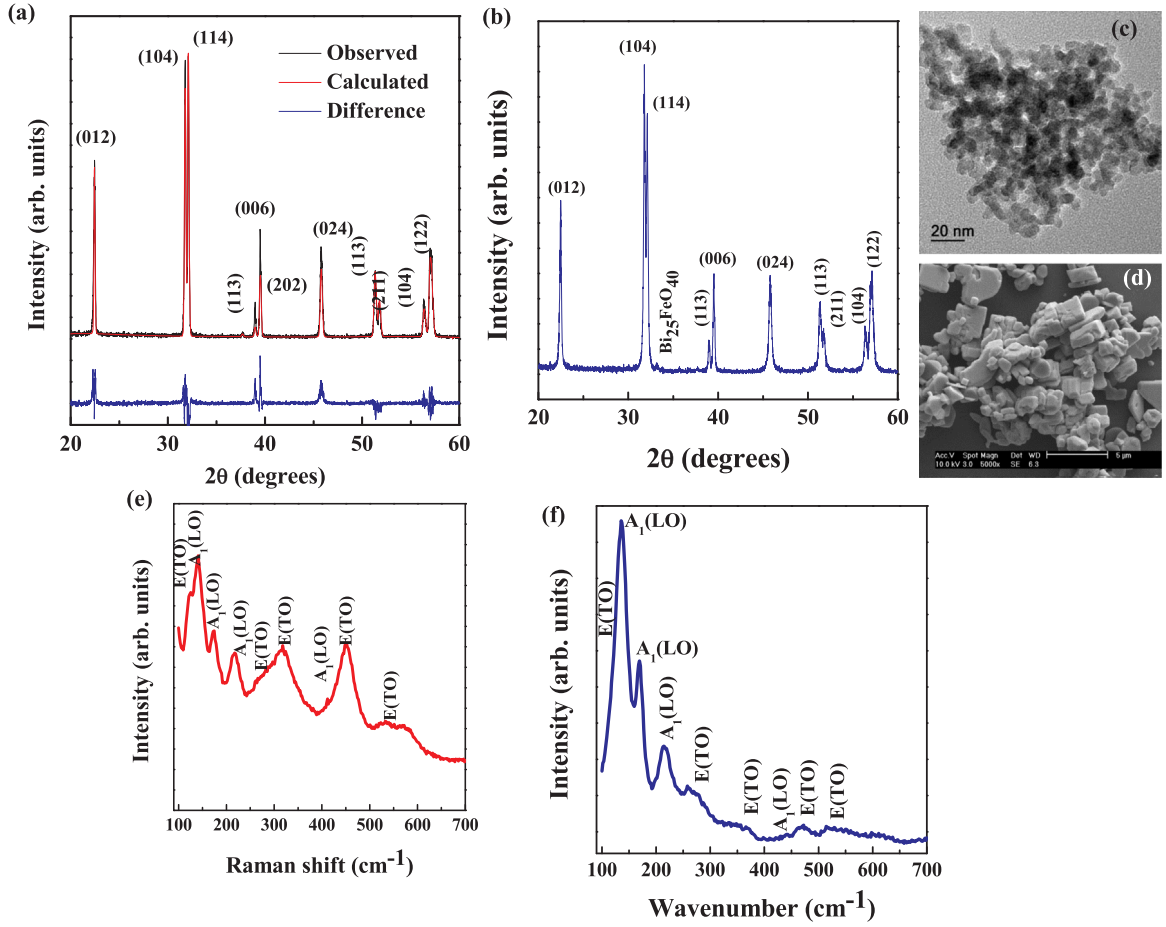

Fig. 1. (a) Rietveld refined XRD patterns of pure BFO bulk powders recorded at Room temperature. BFO is found to form in perovskite structure. (b) XRD patterns of pure BFO nanoparticles recorded at Room temperature. (c) SEM image of BFO particles indicating the micron size particles. (d) High resolution TEM image of BFO nanoparticles indicating the nano size particles. (e) Raman spectra of BFO powders and (f) nanoparticles recorded at room temperature indicating the presence of A and E modes.

Recently Xia et al. [29] have explored the possibility of using BFO thin films grown on stainless steel as a anode material for LIB's and cycled only upto 50 cycles. BFO exhibits theoretical specific capacity of BFO is 770 mAh/g and it has ability to store an immense amount of Li. There is no report on electrochemical properties of BFO nanoparticles as well as bulk materials and exploring the possibilities of utilizing them as an anode for Na-ion batteries. The current work was executed on the systematic growth and surface morphology and exploring the correlation of morphology changes and electrochemical characteristics of $BiFeO_3$ nanoparticles and bulk material prepared by sol-gel and hydrothermal method respectively. Utilizing BFO bulk and nanomaterials as anode material for SIB's is discussed for the first time. Obtained structural and electrochemical results are discussed and presented in this paper.

2. Experimental

Hydrothermal method was employed to prepare the bulk BFO material. Bi $(NO_3)_3{\cdot}5H_2O$, $FeCl_3$ and NaOH with 99.99% pure chemicals were used as a starting materials. The initial precursor was prepared by mixing mol of Bi$(NO_3)_3{\cdot}5H_2O$ and mol of $FeCl_3$ dissolved in 50 ml acetone. The well mixed solution was added into 200 ml distilled (DI) water and ammonia solution were added drop by drop under stirring until the pH value of the solution reached 11. After 20 min of stirring, the mixture was washed and filtered with DI water and ethanol. The co-precipitate was re-dispersed in 40 ml of DI water and 8 g of NaOH was added into the suspension under stirring. Obtained solution was poured into 200 ml Teflon-lined vessel with two third filling of its volume for further hydrothermal reaction. The Teflon autoclaves were airtight closed and retained at 140 °C for 40 h in a heat control oven. After completion of hydrothermal reaction, the Teflon autoclaves were cool down to ambient temperature. The end product (BFO powder) was gathered and washed several times with acetone, DI water and ethanol to wash out the unwanted ions, and then dried overnight in an oven at 70° C. $BiFeO_3$ nanoparticles were prepared employing the following procedure. 0.5 mol Bi $(NO_3)_3{\cdot}5H_2O$ was first dissolved in ethylene glycol with continuous stirring to get a transparent solution. Then 0.5 mol Fe $(NO_3)_3{\cdot}9H_2O$ was slowly added into the above mentioned transparent solution. After stirring the solution for 30 min, brownish red colloidal sol was obtained. The sol was dried at 90 °C for 28 h and the $BiFeO_3$ xerogel powder was seen to form. The xerogel was heat treated in air at 400 °C for 30 min to remove organic compounds. Subsequently, the remained powders were annealed at 500 °C for 30 min to get the $BiFeO_3$ nanoparticles. The synthesized BFO powders were studied employing an Cu K_α (λ = 0.15406 nm) X-ray diffractometer (XRD, Rigaku, D/MAX-IIIC X-ray diffractometer, Tokyo, Japan). The surface morphology and particle size of BFO powders were characterized employing a field emission scanning electron microscope (FE-SEM Philips XL30 FEG, Eindhoven, Netherland). Particle size and morphology analysis of BFO nanoparticles were characterized employing a Transmission electron microscope (TEM), JEOL 2010F HRTEM, Japan, with a 200 kV operating voltage. The Raman spectra of BFO bulk and nanoparticles were acquired employing a HR 800 Raman spectrophotometer (Jobin Yvon- Horiba, France) employing monochromatic He-Ne LASER (632.8 nm), operating at 20 mW.

The electrochemical studies of the $BiFeO_3$ bulk and nanomaterials

Table 1
Results or Rietveld refinement such as Bond angles and bond length values of $BiFeO_3$.

Compound	O – Bi – O	O – Fe – O	Bi-O-Fe	Bond length (Å)		
	Bond angle (± 0.001 degrees)	Bond angle (± 0.001 degrees)	Bond angle (± 0.001 degrees)	Fe-O	Fe-Bi	Bi-O
$BiFeO_3$	74.231	118.361	115.921	2.165	3.306	2.731

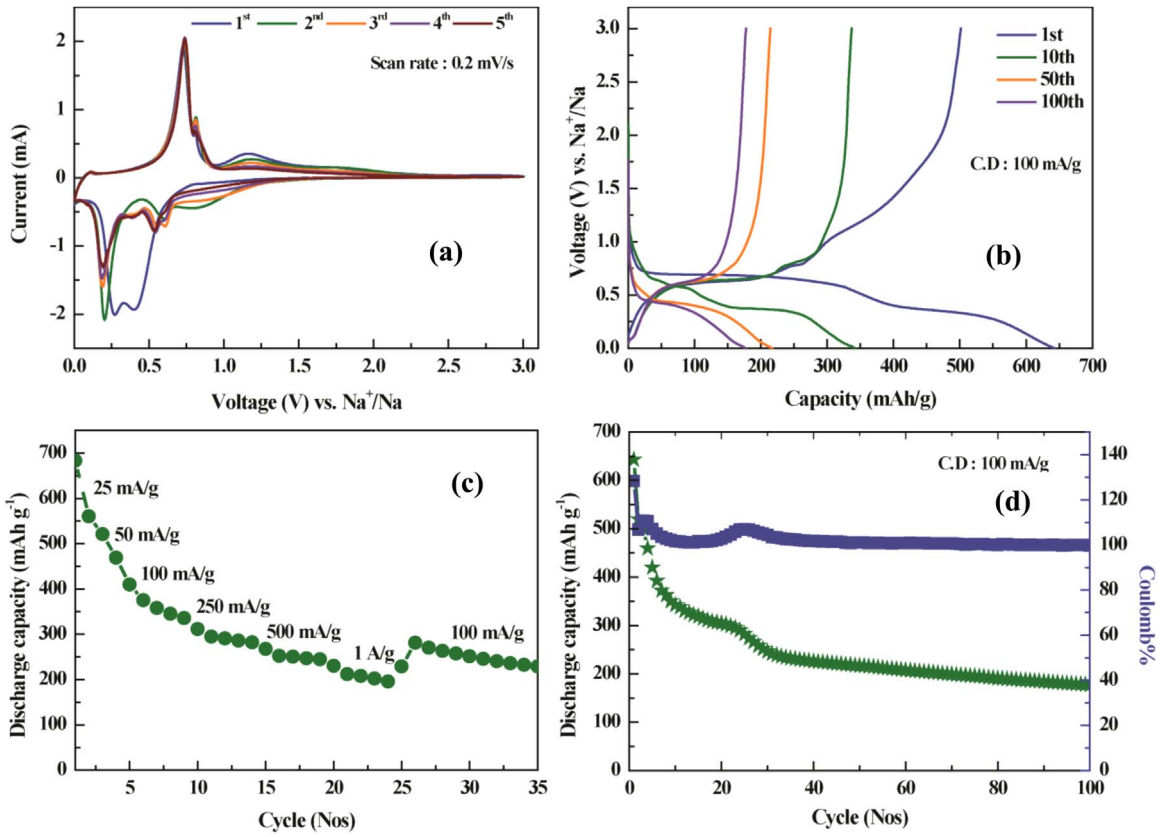

Fig. 2. (a) Cyclic voltammetry plots for the BFO powders with alginate binder (b) charge/discharge plots for the BFO powders with Na-alginate binder at 100 mA/h current rate. (c) Cyclic performance of BFO powders at different current rates. (d) Discharge capacity and coulombic efficiency of BFO powders till 100th cycle.

were carried out employing CR2032 coin cells. The slurry was prepared by mixing $BiFeO_3$, conducting carbon (Super P carbon black) and Na alginate binder with 70:20:10 ratios in DI water. Slurry was ground in mortar pestle for two hours to get the uniformity and deposited on an Al foil using doctor blade. Coated Al foil was dried for 12 h in a vacuum oven and then made into 12 mm diameter electrodes. Na metal pieces were cut into foil and then employed as an anode. Mixture of 1 M $NaClO_4$ solution and $CH_3C_2H_3O_2CO$ (propylene carbonate) was employed as a liquid electrolyte and Borosilicate fibers were used as a separator. All the coin cells for electrochemical studies were fabricated inside the glove box which was filled with Ar. The cyclic voltammetry (CV) measurements were carried out employing Biologic Science Instruments (Model: VMP3) in the voltage range 0–3 V. Charge discharge between 0 and 3 V at different C rates were measured employing a VMP3 Bio-Logic potentiostat.

3. Results and discussion

Fig. 1(a) shows the observed and calculated XRD patterns of the BFO bulk powders along with the difference after the Rietveld refinement was carried out. GSAS program was employed to refine the XRD pattern of BFO bulk material acquired at room temperature. The fitting parameters such as weighted refined parameter (wrp) and the goodness of the fit (χ^2) values are 3% and 1.00 respectively. BFO is seen to crystalize in perovskite (rhombohedrally distorted) structure correspond to R3c space group [30]. Biasotto et al. [31] have reported the rapid hydrothermal microwave method to synthesize high quality $BiFeO_3$ nanoparticles at low temperatures with very less preparation time (1 h) [30]. In the present case, no impurity peaks are identified in XRD data, indicating the good quality of the BFO power. Diffraction peaks are seen to be very sharp at RT, shows the well-crystallized BFO material. The lattice constants *a*, *b* and *c* values calculated from refinement for BFO sample at RT is 5.573, 5.573 and 13.854 Å (± 0.002 Å) respectively. The bond angles and bond lengths at different atomic sites are given in the Table 1. Fig. 1(b) shows the XRD patter of BFO nanoparticles prepared by sol-gel method, which is also seen to crystalize in perovskite (rhombohedrally distorted) structure (with very small amount of $Bi_{25}FeO_{40}$ impurities) belonging to *R3c* space group. SEM image of as prepared BFO particles is depicted in Fig. 1(c) and it exhibits polygon surface with the average size of ~7–8 μm. Fig. 1(d) shows the high resolution TEM image of BFO nanoparticles, indicating uniform nanoparticles with average of 10 nm size. Fig. 1(e) and (f) shows the Raman spectra for BFO bulk powders and nanoparticles respectively, measured at RT. The obtained Raman modes can be assigned to E and A longitudinal (LO) and transverse (TO) modes [31,32]. The peaks appear at 270, 295, 348, 371, 440, and

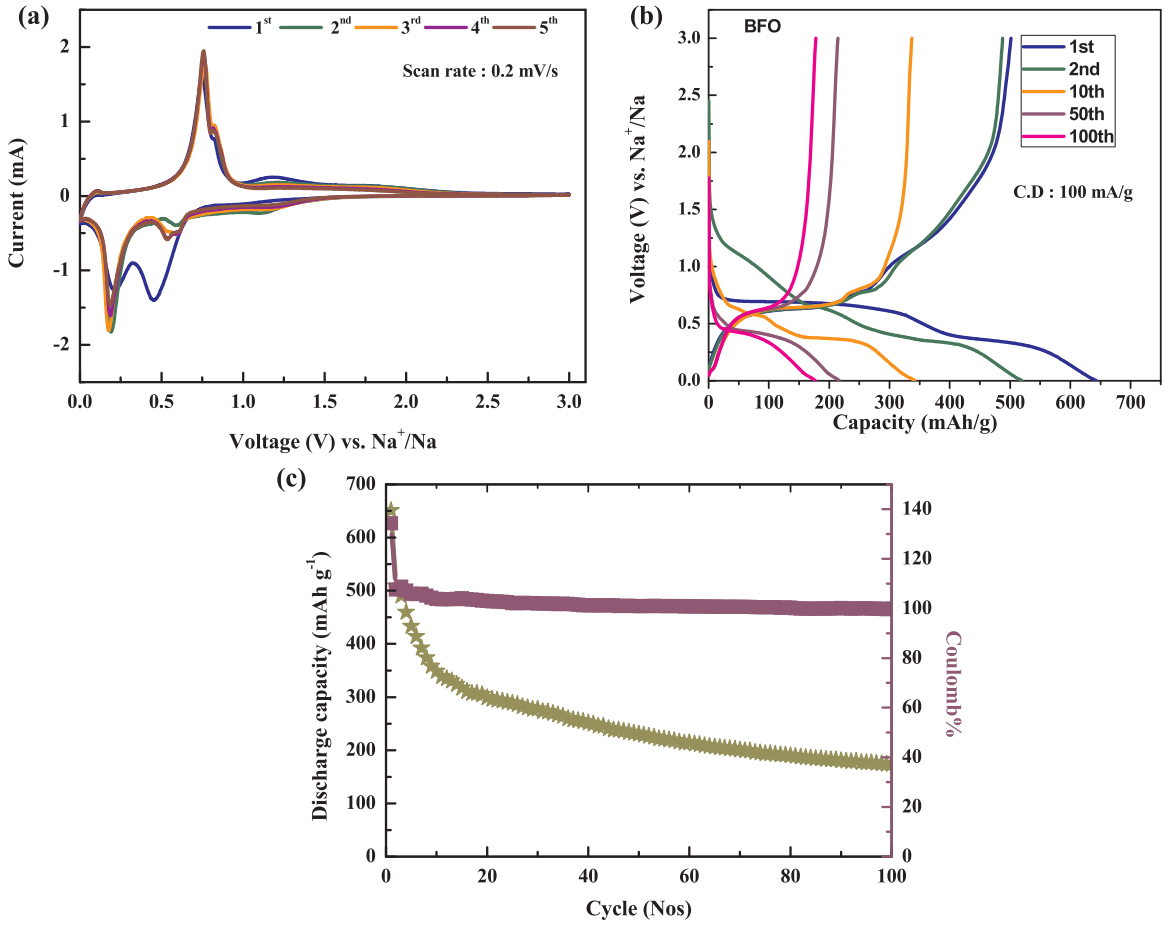

Fig. 3. (a) Cyclic voltammetry plots for the BFO nanoparticles with alginate binder (b) charge/discharge plots for the BFO nanoparticles with Na-alginate binder at 0.1 C current rate. (c) Discharge capacity and coulombic efficiency of BFO nanoparticles till 100th cycle.

Table 2
Comparison of physical properties of $BiFeO_3$ material prepared by hydrothermal and sol-gel method.

Parameter	BFO prepared by Hydrothermal method	BFO prepared by Sol-gel method
Lattice constant	$a = b = 5.573$ and $c = 13.854$ Å (± 0.002 Å)	$a = b = 5.571$ and $c = 13.852$ Å (± 0.002 Å)
Average particle size	7–8 μm	10 nm
Discharge capacity at 100th cycle	180 mAh/g	175 mAh/g
Discharge capacity at 50th cycle	220 mAh/g	230 mAh/g

524 cm^{-1} are belongs to the E modes. Peaks at 124, 144, 173 and 210 cm^{-1} are due to the presence of A modes. The peak (A mode) around 124 cm^{-1} can be allocated to the vibrations of Bi-O bonds. Motion of O atoms give raise to the E mode around 270 cm^{-1} and the vibrations of Fe-O bonds resulted in A mode around 152 cm^{-1}. The magnetoelectric coupling (coupling between electric and magnetic dipoles) can be confirmed from the A mode around 144 cm^{-1}, agreeing well with the reports [32,33].

Fig. 2(a) shows cyclic voltammetry (CV) schemes of BFO bulk material for 5 cycles scanning at 0.2 mV/s rate. First, the cell was discharged from open circuit voltage to 0.2 V and charged to 3 V. During first discharge, broad peak at about 0.3 V is observed. From the first charge and the remaining cycles, sharp peaks at 0.7, 1.2 V (During Charging) and 0.5 and 0.2 V (During discharging) are observed. All through at the 1st discharge, BFO reacts with the sodium ions and perovskite structure might be destroyed and converts into Bi and Fe metal particles and amorphous Na_2O phase.

First Conversion redox mechanism can be stated as:

$$BiFeO_3 + 6Na^+ + 6e^- \rightarrow Bi + Fe + 3\,Na_2O \text{ —} \quad (1)$$

From the first charge and the second cycle, two distinguished peaks are observed due to two stages of alloying process among Na and Bi, which can be expressed as.

$$Bi + Na^+ + e^- \rightarrow NaBi \text{ ——} \quad (2)$$

$$NaBi + 2Na^+ + 2e^- \rightarrow Na_3Bi \text{ ——} \quad (3)$$

To explore the cycle ability of the BFO bulk material, 100 cycles of charge/discharge were carried out in the voltage rage between 0 and 3Vat the rate of 100 mA/g and is shown in Fig. 2(b). The specific capacity of BFO bulk material is seen to decrease gradually from 650 mAh/g to 220 mAh/g after 50 cycles and then the capacity fading takes place very slowly till 100th cycle. After 100 cycles, the discharge capacity of BFO is seen to be 180 mAh/g. The discharge capacity of BFO material at different current rates of 25 mA/g, 50 mA/g, 100 mA/g, 250 mA/g, 500 mA/g and 1 A/g for 35 cycles is shown in Fig. 2(c). When the BFO electrode is cycled at a rate of 25 mA/g, it exhibits the discharge capacity of 700 mA/g at first cycle. Subsequently, the discharge rate is increased stepwise to 1 A/g and capacity is seen to decrease gradually to 200 mAh/g. After 25 cycles, the current rate being

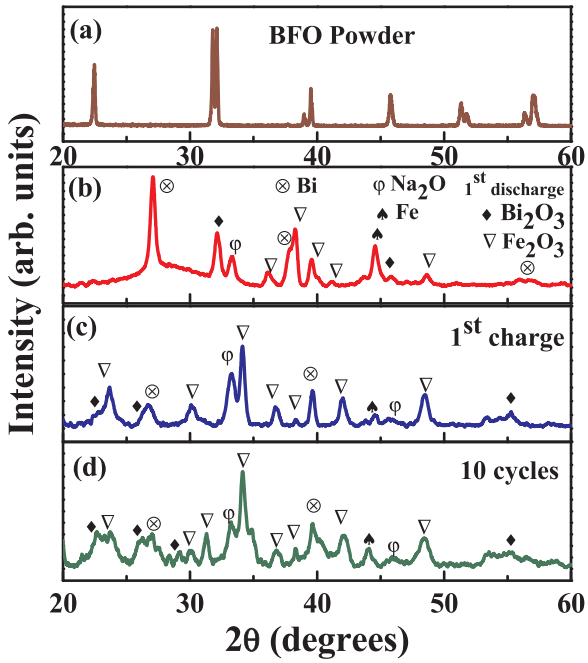

Fig. 4. XRD pattern of (a) BFO powder (b) after 1st discharge (c) after 1st charge and (d) after 10 cycles.

again decreased to 100 mAh/g, capacity seen to increase to 350 mAh/g and this value also decreases marginally till 35th cycle. Fig. 2(d) shows the cycling performance of BFO material with Na alginate binder and it indicates that the BFO material provide an initial discharge capacity of 700 mAh/g at 100 mA/g (0.1 C), and the discharge capacity is seen to be 180 mAh/g after 100 cycles. Coulombic efficiencies (Charge capacity/discharge capacity) of BFO electrode during the 100 cycles are all around 100%, except the very first cycle.

Nanoparticles of cathode and anode materials of LIB's and SIB's are reported to exhibit better electrochemical performance and show stable capacity compared to that of bulk materials due to short Li/Na diffusion length and more surface area. In the present case, in order to overcome the capacity fading of BFO bulk material, electrochemical performance of BFO nanoparticles were carried out. Cyclic voltammetry and charge discharge at 0.1 C rate was performed and the results are shown in Fig. 3(a) and (b) respectively. First, the cell was discharged from open circuit voltage to 0.2 V and charged to 3 V and subsequently cycled 5 times between 0.2–3 V. CV of BFO nanoparticles exhibits redox peaks at the same position as bulk BFO shows. From the 2nd cycle to 5th cycle, CV of BFO nanoparticles is very stable and the area under the curve is almost same. To explore the possible stability of cycle performance of the BFO nanoparticles, 100 cycles of charge/discharge were performed in the voltage rage between 0 and 3Vat the rate of 100 mA/g and is shown in Fig. 3(b). The specific capacity of BFO nanoparticle is seen to decrease gradually from 675 mAh/g to 230 mAh/g after 50 cycles and then the capacity fading takes place very slowly till 100th cycle. After 100 cycles, the discharge capacity of BFO nanoparticle is seen to be 175 mAh/g. Nanoparticles of BFO is not seen to stabilize the capacity

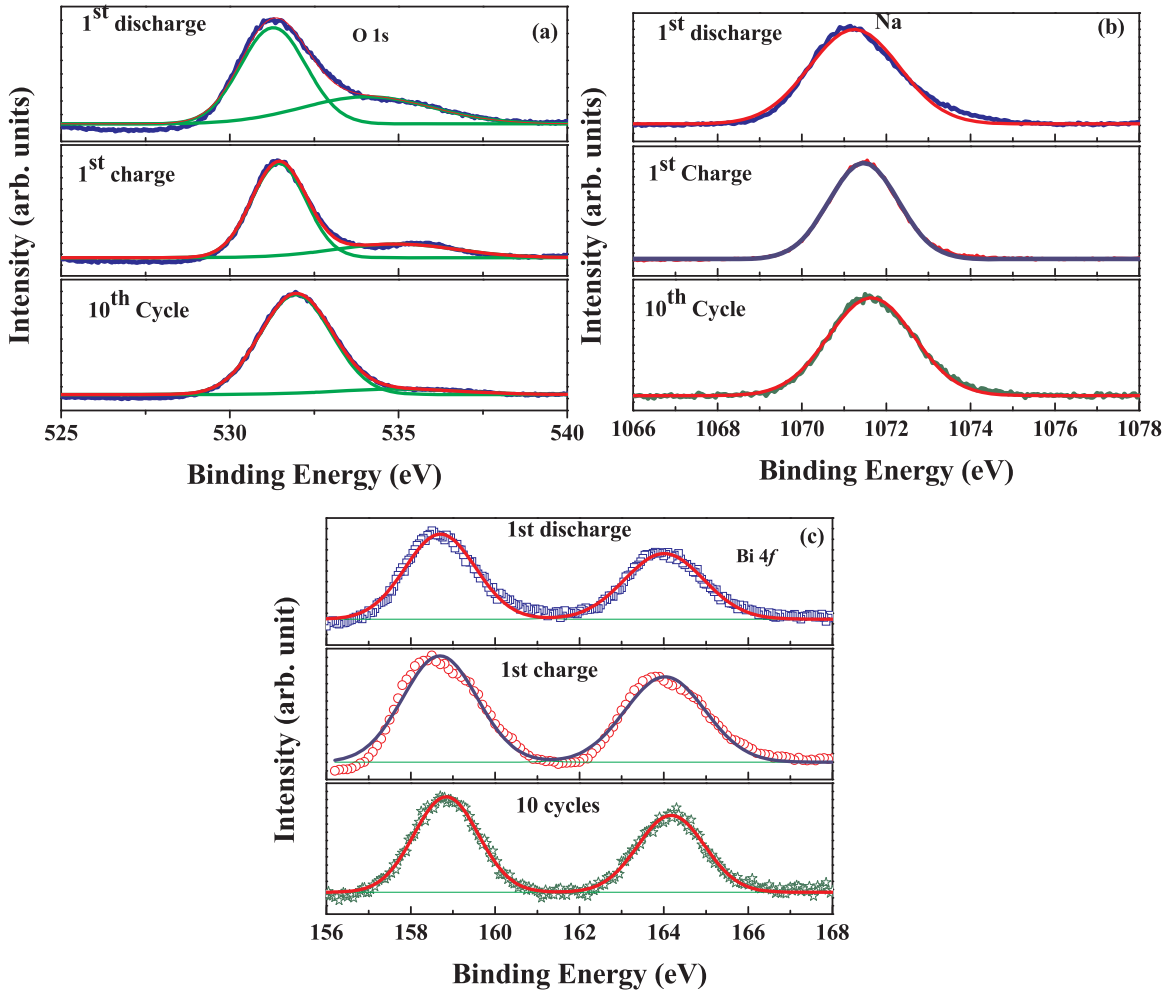

Fig. 5. XPS Spectra of (a) O 1*s*, (b) Na 1*s* and (c) Bi 4*f* of BFO powder after 1st discharge, after 1st charge and after 10 cycles.

fading. BFO nanomaterial with some other morphology (nanowires, nanorods) and/or adding some additives (Ex: Al_2O_3) might improve the capacity fading effect in BFO, which can be explored as a continuation of the present work. Fig. 3(c) shows the cycling performance of BFO nanoparticles with Na alginate binder and it indicates that the BFO nanoparticles provide an initial discharge capacity of 675 mAh/g at 100 mA/g (0.1 C), and the discharge capacity is seen to be 175 mAh/g after 100 cycles which is almost similar to the bulk BFO. Table 2 shows the specific capacity of BFO bulk and nanoparticles at various cycles. Coulombic efficiencies (Charge capacity/discharge capacity) of BFO electrode during the 100 cycles are all around 100%, except the very first cycle. Graphite anode is used in most of the commercially available Li batteries. Theoretical capacity of graphite anode is 372 mAh/g, which is low value and needs to be improved. Oxide materials such as Fe_2O_3, Co_3O_4, MnOx and CuO are reported to have theoretical capacity of 1007, 890, 700 and 674 mAh/g respectively. All such material is in research level and yet to be commercialized. $BiFeO_3$ has theoretical capacity of 770 mAh/g and in the present case; we have observed the capacity of 650 mAh/g at first cycle. High initial capacity of $BiFeO_3$ gives an indication that it can be utilized as an anode component for Na ion batteries after stabilizing the capacity fading.

In order to understand the structural changes of BFO electrode after the electrochemical cycles, ex-situ XRD and XPS characterizations were performed on the cycled BFO electrodes after first discharge, first cycle and after ten cycles and compared with as prepared BFO powder (Fig. 4). Electrochemically cycled coin cells were opened in Ar filled glow box to get the reacted electrodes and dried within the glow box for one day. Dried electrodes were carried out to the XRD measurement in an Ar filled box and the measurements were carried out to avoid any reaction with atmosphere. After first discharge Fig. 4(b), BFO perovskite structure is completely destroyed and it contains Bi, Fe, Fe_2O_3, Bi_2O_3 and Na_2O phases. XRD pattern of electrodes after first cycle (Fig. 4(c)) and 10th cycle (Fig. 4(d)) also contain Fe_2O_3 (α and γ phases), Bi_2O_3, Fe, Bi and Na_2O phases.

Fig. 5(a) illustrates the O 1*s* XPS spectra of BFO cathodes (electrodes) after 1st discharge, 1st cycle and after 10 cycles respectively indicating a slightly distorted peak at ~ 531 eV. Along with the O 1*s* peak, small additional peak around 536 eV is also observed for all the cycled electrodes in the spectra. The peak at low binding energy for all the cycled electrodes can be attributed to the O1*s* band and the small peak present at right side (higher binding energy) of O 1*s* is in commonly ascribed with the presence of oxygen vacancy in the BFO sample [34]. BFO samples prepared employing hydrothermal method at low temperatures is reported to have oxygen vacancy and the present observation also agrees well with the reports [34]. Fig. 5(b) shows Na 1s core level XPS spectra at 1071.15, 1071.45 and 1071.5 eV of electrodes after 1st discharge, 1st cycle and after 10 cycles respectively. The Na 1*s* photoelectron binding energy is reported to be in between 1070 eV and 1075 eV [35]. Presence of Na peaks in all the three cycled electrodes confirm the sodiation/desodiation in all the electrodes. Fig. 5(c) displays the Bi 4*f* XPS spectra of BFO electrodes after 1st discharge, 1st cycle and after 10 cycles confirming couple of peaks as a result of Bi-O bonds. Bismuth 4*f* doublet containing of two peaks concentrated at ~158 and ~164 eV can be seen for all the electrodes, agreeing with the previous reports [36].

4. Conclusion

In summary, Pure $BiFeO_3$ bulk material and nanoparticles were successfully prepared by hydrothermal and sol-gel process respectively. The structural and morphological properties of as prepared $BiFeO_3$ material were examined by XRD, SEM and Raman spectroscopy methods. $BiFeO_3$ nanoparticles as well as the bulk material with alginate binder delivers initial capacity around 650 mAh/g and gradually decreases to ~200 mAh/g at 100th cycle at 0.1 C rate. Conversion and alloying process during electrochemical cycles are investigated using cyclic voltammetry ex-situ XRD and XPS measurements.

References

[1] S. Karaal, H. Köse, A.O. Aydin, H. Akbulut, The effect of $LiBF_4$ concentration on the discharge and stability of $LiMn_2O_4$ half cell Li ion batteries, Mater. Sci. Semicond. Process. 38 (2015) 397–403.

[2] S. Takeuchi, H. Tan, K. Kamala Bharathi, G.R. Stafford, J. Shin, S. Yasui, I. Takeuchi, L.A. Bendersky, Epitaxial $LiCoO_2$ films as a model system for fundamental electrochemical studies of positive electrodes, ACS Appl. Mater. Interfaces 7 (2015) 7901–7911.

[3] J.B. Goodenough, Y. Kim, Challenges for rechargeable Li batteries, Chem. Mater. 22 (2010) 587–603.

[4] N.S. Choi, Z.H. Chen, S.A. Freunberger, X.L. Ji, Y.K. Sun, K. Amine, G. Yushin, L.F. Nazar, J. Cho, P.G. Bruce, Challenges facing lithium batteries and electrical double-layer capacitors, Angew. Chem. Int. Ed. 51 (2014) 9994–10024.

[5] Y. Oumellal, A. Rougier, G.A. Nazri, J.M. Tarascon, L. Aymard, Metal hydrides for lithium-ion batteries, Nat. Mater. 7 (2008) 916–921.

[6] S.W. Kim, D.H. Seo, X. Ma, G. Ceder, K. Kang, Electrode materials for rechargeable sodium-ion batteries: potential alternatives to current lithium-ion batteries, Adv. Energy Mater. 2 (2012) 710–721.

[7] D. Kim, S.H. Kang, M. Slater, S. Rood, J.T. Vaughey, N. Karan, M. Balasubramanian, C.S. Johnson, Enabling sodium batteries using lithium-substituted sodium layered transition metal oxide cathodes, Adv. Energy Mater. 1 (2011) 333–336.

[8] Y.N. Ko, S.H. Choi, Y.C. Kang, Hollow cobalt selenide microspheres: synthesis and application as anode materials for Na-ion batteries, ACS Appl. Mater. Interfaces 8 (2016) 6449–6456.

[9] V. Palomares, P. Serras, I. Villaluenga, K.B. Hueso, J. Carretero- Gonzalez, T. Rojo, Na-ion batteries, recent advances and present challenges to become low cost energy storage systems, Energy Environ. Sci. 5 (2012) 5884–5901.

[10] H. Pan, Y.S. Hu, L. Chen, Room-temperature stationary sodium-ion batteries for large-scale electric energy storage, Energy Environ. Sci. 6 (2013) 2338–2360.

[11] B. Jache, P. Adelhelm, Use of graphite as a highly reversible electrode with superior cycle life for sodium-ion batteries by making use of Co-intercalation phenomena, Angew. Chem. Int. Ed. 53 (2014) 10169–10173.

[12] W.P. Sun, X.H. Rui, J.X. Zhu, L.H. Yu, Y. Zhang, Z.C. Xu, S. Madhavi, Q.Y. Yan, Ultrathin nickel oxide nanosheets for enhanced sodium and lithium storage, J. Power Sources 274 (2015) 755–761.

[13] S. Hariharan, K. Saravanan, P. Balaya, α-MoO_3: a novel high performance anode material for sodium-ion batteries, Electrochem. Commun. 31 (2013) 5–9.

[14] Y.Z. Jiang, M.J. Hu, D. Zhang, T.Z. Yuan, W.P. Sun, B. Xu, M. Yan, Transition metal oxides for high performance sodium ion battery anodes, Nano Energy 5 (2014) 60–66.

[15] S. Komaba, T. Mikumo, N. Yabuuchi, A. Ogata, H. Yoshida, Y. Yamada, Electrochemical insertion of Li and Na ions into nanocrystalline Fe_3O_4 and γ-Fe_2O_3 for rechargeable batteries, J. Electrochem. Soc. 157 (2010) A60–A65.

[16] N. Li, S. Liao, Y. Sun, H.W. Song, C.X. Wang, Uniformly dispersed self-assembled growth of Sb_2O_3/Sb@Graphene nanocomposites on a 3D carbon sheet network for high Na-storage capacity and excellent stability, J. Mater. Chem. A 3 (2015) 5820–5828.

[17] X.S. Zhou, X. Liu, Y. Xu, Y.X. Liu, Z.H. Dai, J.C. Bao, An SbO_x/reduced graphene oxide composite as a high-rate anode material for sodium-ion batteries, J. Phys. Chem. C 118 (2014) 23527–23534.

[18] Q. Sun, Q.Q. Ren, H. Li, Z.W. Fu, High capacity Sb_{2O4} thin film electrodes for rechargeable sodium battery, Electrochem. Commun. 13 (2011) 1462–1464.

[19] M. Shimizu, H. Usui, H. Sakaguchi, Electrochemical Na-insertion/extraction properties of SnO thick-film electrodes prepared by gas-deposition, J. Power Sources 248 (2014) 378–382.

[20] Z. Hu, L.X. Wang, K. Zhang, J.B. Wang, F.Y. Cheng, Z.L. Tao, J. Chen, MoS_2 nanoflowers with expanded interlayers as high-performance anodes for sodium-ion batteries, Angew. Chem. Int. Ed. 53 (2014) 12794–12798.

[21] Y. Sun, L. Zhao, H.L. Pan, X. Lu, L. Gu, Y.S. Hu, H. Li, M. Armand, Y. Ikuhara, L.Q. Chen, X.J. Huang, Direct atomic-scale confirmation of three-phase storage mechanism in Li4Ti5O12 anodes for room-temperature sodium-ion batteries, Nat. Commun. 4 (2013) 1870–1879.

[22] B.R. Lee, E.-S. Oh, Effect of molecular weight and degree of substitution of a sodium-carboxymethyl cellulose binder on $Li_4Ti_5O_{12}$ anodic performance, J. Phys. Chem. C 117 (2013) 4404–4409.

[23] L.M. Wu, D. Buchholz, D. Bresser, L.G. Chagas, S. Passerini, Anatase TiO_2 nanoparticles for high power sodium-ion anodes, J. Power Sources 251 (2014) 379–385.

[24] M.D. Rossell, R. Erni, M.P. Prange, J.C. Idrobo, W. Luo, R.J. Zeches, S.T. Pantelides, R. Ramesh, Atomic structure of highly strained $BiFeO_3$ thin films, Phys. Rev. Lett. 108 (2012) (047601-04605).

[25] T. Choi, S. Lee, Y.J. Choi, V. Kiryukhin, S.W. Cheong, Switchable ferroelectric diode and photovoltaic effect in $BiFeO_3$, Science 324 (2009) 63–66.

[26] S.Y. Yang, J. Seidel, S.J. Byrnes, P. Shafer, C.H. Yang, M.D. Rossell, P. Yu, Y.H. Chu, J.F. Scott, J.W. Ager, L.W. Martin, R. Ramesh, Above-bandgap voltages from ferroelectric photovoltaic devices, Nat. Nanotechnol. 5 (2010) 143–147.

[27] J. Wu, Z. Fan, D. Xiao, J. Zhu, J. Wang, Multiferroic bismuth ferrite-based materials for multifunctional applications: ceramic bulks, thin films and nanostructures, Progress. Mater. Sci. 84 (2016) 335–402.

[28] L.V. Costa, L.S. Rocha, J.A. Cortés, M.A. Ramirez, E. Longo, A.Z. Simões, Enhancement of ferromagnetic and ferroelectric properties in calcium doped BiFeO3 by chemical synthesis, Ceram. Int. 41 (2015) 9265–9275.

[29] H. Xia, F. Yang, M. On Lai, L. Lu, W. Song, Electrochemical properties of $BiFeO_3$ thin

films prepared by pulsed laser deposition, Funct. Mater. Lett. 2 (2009) 163–167.
[30] P. Singh, J.H. Jung, Effect of oxygen annealing on magnetic, electric and magnetodielectric properties of Ba-doped $BiFeO_3$, Physica B 405 (2010) 1086.
[31] G. Biasotto, A.Z. Simoes, C.R. Foschini, M.A. Zaghete, J.A. Varela, E. Longo, Microwave-hydrothermal synthesis of perovskite bismuth ferrite nanoparticles, Mater. Res. Bull. 46 (2011) 2543–2547.
[32] M.K. Singh, H.M. Jang, S. Ryu, M.H. Jo, Polarized Raman scattering of multiferroic $BiFeO_3$ epitaxial films with rhombohedral *R3c* symmetry, Appl. Phys. Lett. 88 (2006) 042907–042909.
[33] P.C. Sati, M. Arora, S. Chauhan, S. Chhoker, M. Kumar, Structural, magnetic, and optical properties of Pr and Zr Codoped $BiFeO_3$ multiferroic ceramics, J. Appl. Phys. 112 (2012) 094102.
[34] L. Fang, J. Liu, S. Ju, F. Zheng, W. Dong, M. Shen, Experimental and theoretical evidence of enhanced ferromagnetism in sonochemical synthesized $BiFeO_3$ nanoparticles, Appl. Phys. Lett. 97 (2010) (242501-24503).
[35] T.G. Deepak, D. Subash, G.S. Anjusree, K.R. Narendra Pai, S.V. Nair, A.S. Nair, Photovoltaic property of anatase TiO_2 3-D mesoflowers, ACS Sustain. Chem. Eng. 2 (2) (2014) 2772–2780.
[36] F. Gao, C. Cai, Y. Wang, S. Dong, X.Y. Qiu, G.L. Yuan, Z.G. Liu, J.M. Liu, Preparation of La-doped $BiFeO_3$ thin films with Fe^{2+} ions on Si substrates, J. Appl. Phys. 99 (2006) 094105.